Physically Informed Graph-based Deep Reasoning Net for Efficient Combinatorial Phase Mapping

Yimeng Min†
Computer Science
Cornell University
Ithaca, USA
ym499@cornell.edu

Ming-Chiang Chang†
Materials Science and Engineering
Cornell University
Ithaca, USA
mc2663@cornell.edu

Shufeng Kong*
Software Engineering
Sun Yat-sen University
Guangzhou, China
sk2299@cornell.edu

John M. Gregoire
Liquid Sunlight Alliance
California Institute of Technology
Pasadena, USA
gregoire@caltech.edu

R. Bruce van Dover
Materials Science and Engineering
Cornell University
Ithaca, USA
vandover@cornell.edu

Michael O. Thompson
Materials Science and Engineering
Cornell University
Ithaca, USA
mot1@cornell.edu

Carla P. Gomes
Computer Science
Cornell University
Ithaca, USA
gomes@cs.cornell.edu

***Abstract*—Phase mapping is a crucial challenge in materials discovery, which entails determining crystalline phase distribution in condition space based on a collection of X-ray diffraction (XRD) data. This task involves exploring the space of potential phases, identifying existing phases, and determining their respective weight distribution in the condition space while adhering to strict physics constraints. In recent years, there has been a growing interest in leveraging machine learning (ML) techniques to tackle the phase mapping problem. ML methods offer the potential to handle larger and more complex phase mapping instances and provide enhanced accuracy compared to traditional approaches. Among promising ML approaches, DRNets, which formulates the phase mapping problem as an unsupervised pattern demixing problem, represents the current state of the art. Despite its practical effectiveness, DRNets does have certain limitations. For instance, it employs a single multiplicative factor to calculate the stick locations in XRD patterns, which may not accurately reflect the underlying physics of X-ray diffraction. Additionally, DRNets relies on an expensive path-based schema to enforce phase weight smoothness.**

To overcome these limitations, we propose a novel approach called Physically-informed Graph-based DRNet (PG-DRNet). PG-DRNet incorporates a physical decoder that estimates the crystals' lattice parameters and reconstructs XRD patterns based on Bragg's law. Additionally, we introduce a graph-based schema to enforce phase weight smoothness as well as lattice and peak intensity shift. This graph-based schema provides several advantages, including improved computational efficiency compared to the path-based schema utilized in DRNets. To thoroughly evaluate the effectiveness of our approach, we conducted experiments on various chemical systems. Notably, our evaluation went beyond the scope of previous studies that solely focused on varying compositions and extends to explore the additional dimensions of varying annealing time and temperature conditions. Our results demonstrate that PG-DRNet achieves higher accuracy, lower reconstruction loss and significantly faster performance when compared to DRNet results.

***Index Terms*—phase mapping, unsupervised pattern demixing, physically informed decoding, graph-based smoothness**

I. Introduction

In materials science, a phase is uniquely defined by both its crystal structure and chemical composition. A phase diagram, often referred to as a phase map, provides crucial information about the phases that exist under specific chemical compositions and processing conditions. This diagram serves as a fundamental cornerstone for materials processing. Therefore, how to rapidly construct phase diagrams has been an important research area. The process of constructing phase diagrams for crystalline materials starts by synthesis and processing of materials. It is followed by crystal structure characterizations using X-ray diffraction (XRD), which generates distinctive signals for each phase characterized by multiple peaks and provide insights into the atomic arrangement of the phase. Finally, the analysis of the set of XRD patterns demixes the contribution of different phases and assigns corresponding weights to each phase at each experimental condition. The experimental facet of phase diagram construction has been significantly expedited with the development of high-throughput experimental techniques, e.g. combinatorial synthesis,high-throughput laser annealing and high-throughput XRD techniques [2]–[4] On the other hand, despite several advancements over the past few years, analyzing a set of measured XRD data to construct a phase diagram, also known as phase mapping, has been a critical missing component in the high-throughput materials research [5]–[7] To create an accurate phase diagram from mixed XRD signals, we have to accurately identify the existing phases and spectrally demix all XRD patterns to retrieve the phase distributions in the phase diagram space while following laws of thermodynamics. This has been shown to be a NP-hard problem because the number of possible phase prototype combinations can grow exponentially with data size [8]. Fur-

†: These two authors contributed equally.
*: Shufeng Kong is also affiliated with the Department of Computer Science at Cornell University and is the corresponding author.

1946-0759/23/$31.00 ©2023 IEEE
DOI 10.1109/ICMLA58977.2023.00061

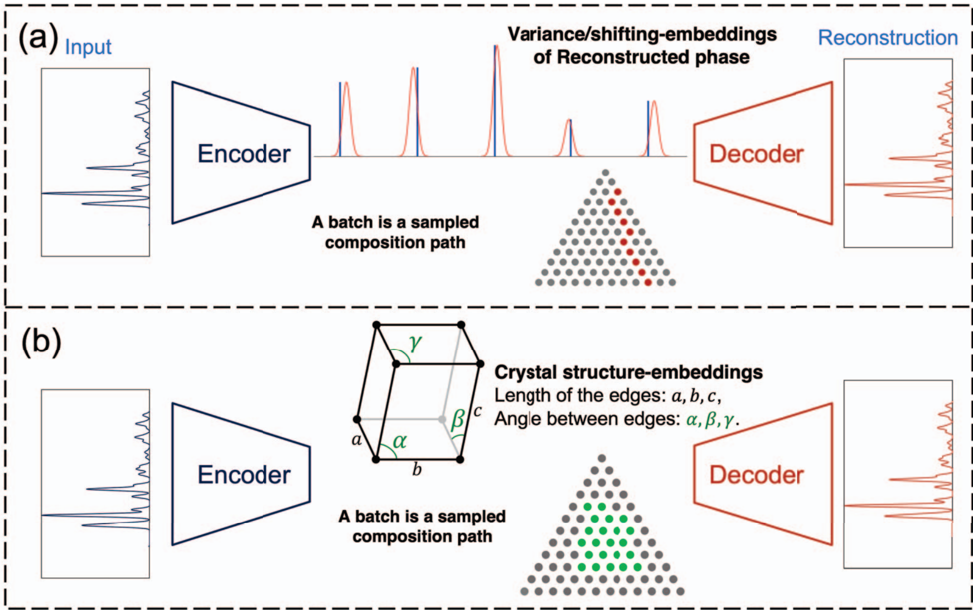

Fig. 1: Illustration of PG-DRNet's framework showcasing the importance of an interpretable structured latent space for incorporating prior knowledge. (a): The original DRNets structure, as proposed in [1], encodes the input XRD pattern into the variance/shifting-embedding of possible phases. (b): PG-DRNet (our model) encodes the input XRD pattern into the lattice parameters of possible phases. This approach provides an interpretable representation that captures essential structural information in the latent space.

thermore, the input XRD data can be contaminated by different kinds of noise, making phase mapping more challenging.

Many phase mapping approaches methods are based on matrix factorization [9]. These methods integrate thermodynamic rules to various extents, such as analyzing the composition graph, integrating demixing with clustering, and incorporating constraint optimization within matrix factorization to enforce thermodynamic rules [5], [10]. However, the use of known prototype patterns in post-processing demixing results often results in a more ill-conditioned demixing outcome.

Recently Chen et al. developed deep reasoning networks (DRNets) [1], which provides the first framework that integrates the enforcement of thermodynamic rules with reasoning about crystal structure prototypes, solving arduous phase mapping problems. The DRNets framework first encodes the input XRD signals to an interpretable latent space and expresses the physical constraints through entropy-based continuous relaxations. Figure 1 shows the pipeline of DRNets. The encoder is composed of 3 three-layer neural networks and the decoder is a generative Gaussian mixture model (GMM) which incorporates prior knowledge about prototype phases of the system. The loss of DRNets consists of two parts: (1) a reconstruction loss between the input data and the generated spectrum; (2) a reasoning loss that captures the domain constraints. The reasoning loss consist of two major constraints: the Gibbs phase rule and the phase field connectivity. However, DRNets uses a path-sampling technique to enforce phase connectivity, which involves generating 100,000 paths per epoch to obtain accurate results. In addition, this large number of paths necessitates a large number of training epochs for convergence.

In this paper, we propose a physically-informed graph-based DRNet (PG-DRNet). Instead of using sampled paths to model the phase field connectivity constraint, PG-DRNet incorporates a graph-based smoothness constraint, PG-DRNet samples different sub-graphs and uses graph smoothness to approximate physical constraints. The comparison between our method and DRNets is shown in Figure 2. The green dots denote the sampled sub-graphs in our model. On the sampled sub-graphs, we use a graph smoothness penalty to encourage the activated phases to form a connective component. More importantly, PG-DRNet incorporates a physical decoder, which allows PG-DRNet to modify the prototype phases more physically and to be adequately expressive. By utilizing the physical decoder, we can extract valuable information regarding the lattice parameters of the crystals present in the XRD data. This additional layer enhances our ability to analyze and interpret the resulting phase diagram, facilitating further analysis and exploration of different material systems.

II. Background

a) The Gibbs phase rule: The Gibbs phase rule, a fundamental concept in thermodynamics, establishes the relationship between the maximum phase count and thermodynamic degrees of freedom. For instance, under constant temperature and pressure, a common assumption in materials science, the Gibbs rule dictates that the number of phases in a ternary chemical system should be at most three. This necessitates a sparse representation of the interpretable latent space, ensuring that each XRD pattern is a mixture of, at most, three basis patterns. In DRNets, the authors first define the entropy function as $-\sum p \log p$ and set the threshold c of sparsity as $\log 3$ to control max phase count, where $p \in \mathbb{R}^m$ is the probability distribution of possible phases in the interpretable latent space, m is the number of candidate prototype phases.

b) Phase field connectivity: Phase field connectivity requires that each phase field form a continuous region in the composition space. This necessitates taking into account the composition graph of the input XRD patterns. In order to embed the connectivity constraint into the reasoning module, DRNets first samples a number of paths in the composition graph and optimizes the objective function using the data points within the sampled paths. Figure 2 (left) shows the scheme of how DRNets models the phase field connectivity constraint. The red points denote a sampled path in the composition space. DRNets penalizes the difference between the phase activation of adjacent data points along the sampled path. However, this can take a huge number of sampled paths to successfully approximate the phase connectivity constraints over the whole composition graph. In fact, for each XRD dataset, DRNets samples 100,000 paths in the composition graph via breadth first search and iteratively applies reasoning to enforce the connectivity rules along the paths. This results in a substantial training cost.

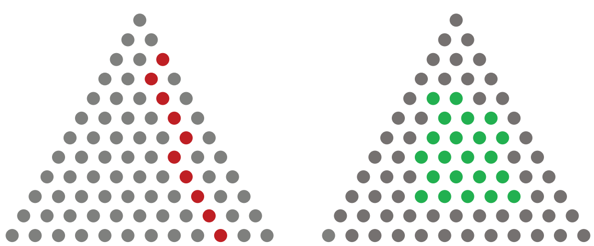

Fig. 2: Different ways of encoding the phase field connectivity constraint in phase mapping. Left: the path-based method used in DRNets. Right: the graph-based method used in PG-DRNet.

III. Method

To model the phase connectivity in PG-DRNet, we utilize smoothness constraints that are based on the generated sub-graphs. These constraints play a crucial role in enforcing a smooth and connected phase distribution. By enforcing sub-graph smoothness, we encourage neighboring data points within sub-graphs to have similar phase assignments and weights.

a) Sampling sub-graphs: In PG-DRNet, the first step in generating sub-graphs is to construct a similarity graph encompassing all samples. This graph is denoted as $\mathcal{G}$ and is created by evaluating the similarity between input samples. For a pair of XRD spectra, S_1 and S_2, with compositions (x_1, y_1) and (x_2, y_2) respectively, we determine if they are connected in $\mathcal{G}$ based on their Euclidean distance. If the distance is smaller than a given threshold, we establish an edge between S_1 and S_2; otherwise, we assume they are not connected in $\mathcal{G}$. We then randomly select a starting point from the composition graph and perform a k-step diffusion along the edges. This diffusion process generates a sub-graph, denoted as $\mathcal{G}'$. By selecting different starting points and varying the number of diffusion steps, we can generate a pool of sub-graphs. This process is illustrated in Figure 3.

During each iteration, we randomly select a sub-graph from the pool and batch the data points within it. This approach effectively captures the connectivity and similarity between the XRD spectra, facilitating the training of PG-DRNet.

b) Building graph smoothness: As mentioned previously, considering n samples and their corresponding XRD patterns $S_{1,2,\ldots,n}$, we construct the similarity graph $\mathcal{G}$ by taking into account the composition, time, and temperature of the input samples. We then define the adjacency matrix $\mathbf{A} \in \mathbb{R}^{n \times n}$ as:

$$\mathbf{A}_{ij} = \begin{cases} 1 & \text{if } S_i \text{ and } S_j \text{ are connected in } \mathcal{G} \\ 0 & \text{otherwise} \end{cases}. \tag{1}$$

Let $\mathbf{L} = \mathbf{D} - \mathbf{A}$ denote the Laplacian matrix of $\mathcal{G}$, where $\mathbf{D}$ is the degree matrix. Given a sub-graph with size l, we first generate a latent space $\mathbf{p} \in \mathbb{R}^{l \times m}$ using the encoder in Figure 1. We then pad the learned latent representation $\mathbf{p}$ with zeros and build a new representation $\mathbf{p}' \in \mathbb{R}^{n \times m}$, where $\mathbf{p}' = [\mathbf{p}'_1 | \mathbf{p}'_2 | \ldots | \mathbf{p}'_m]$, $\mathbf{p}'_i \in \mathbb{R}^n$ is the distribution of i-th phase over the input XRD samples. The smoothness constraint is then defined as:

$$\mathcal{L}_s = \alpha \sum_{i=1}^{m} \frac{\mathbf{p}'^T_i \mathbf{L} \mathbf{p}'_i}{||\mathbf{p}'_i||^2}. \tag{2}$$

After applying eigen-decomposition to the graph Laplacian $\mathbf{L}$, we can rewrite $\mathcal{L}_s$ as $\alpha \sum_{i=1}^{m} \frac{1}{||\mathbf{p}'_i||^2} \mathbf{h}'^T_i (\sum_{j=1}^{n} \lambda_j \mathbf{v}_j \mathbf{v}_j^T) \mathbf{p}'_i = \alpha \sum_{i=1}^{m} \sum_{j=1}^{n} \frac{1}{||\mathbf{p}'_i||^2} \lambda_j |\mathbf{v}_j^T \mathbf{p}'_i|^2$, where $\lambda_1 \leq \lambda_2 \leq \ldots \leq \lambda_n$ are different eigenvalues. When minimizing $\frac{1}{||\mathbf{h}'_i||^2} \sum_{j=1}^{n} \lambda_j |\mathbf{v}_j^T \mathbf{h}'_i|^2$, the smoothness constraint pushes the $\mathbf{h}'_i$ to the eigenstates with low eigenvalues. In other words, $\mathbf{h}'_i$ will have more low frequency components. These low frequency components will encourage local smoothness and promoting the non-zero values $\mathbf{h}'_i$ (activated phases) to be more connected. As an example, Figure 4 shows the composition maps and their corresponding eigenvectors in the Bi-Cu-V system. Lower eigenstates exhibit smooth transitions between different compositions. By pushing the phase distribution towards the lower frequency side, the connectivity constraint is more likely to be satisfied, resulting in a more continuous, connected and therefore more physical phase distribution.

c) Physical decoder: Each peak in the XRD patterns corresponds a family of lattice planes (hkl) with its location in the q space determined by the interplanar distance d_{hkl} through the equation $q_{hkl} = d_{hkl}/2\pi$. In practice, the interplanar distance usually deviates slightly from the reference value in the crystallography database due to non-idealities in the

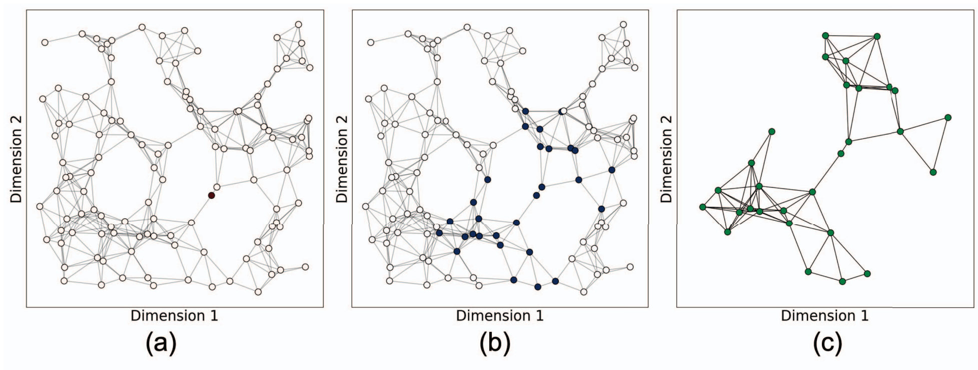

Fig. 3: Illustration of how sub-graphs are built. (a): Select a random start point; (b): After a three-step diffusion from the start point, the diffusion process covers the blue nodes; (c): the resulting sub-graph.

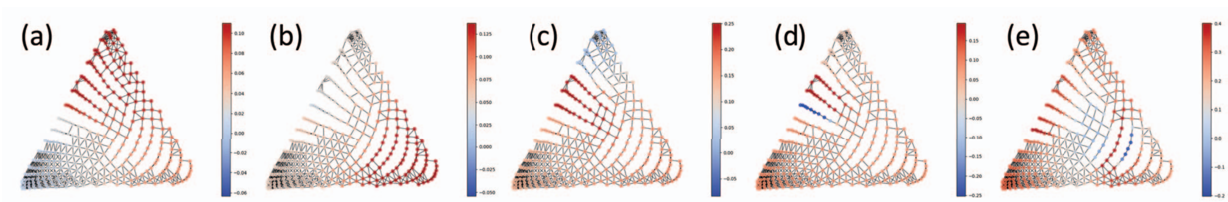

Fig. 4: Different Eigenstates on Bi-Cu-V Graph. (a) to (d): 2nd to 5th eigenstates, (e): 10th eigenstate. The lower eigenstates exhibit smoother transitions.

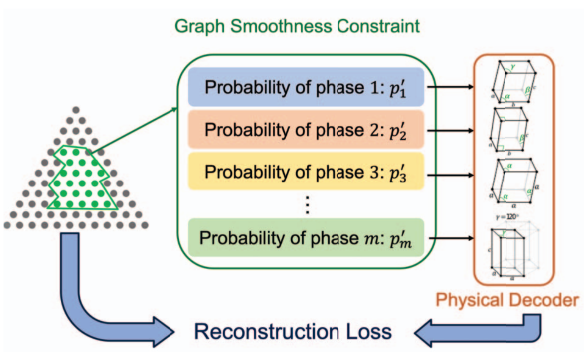

Fig. 5: Illustration of how we combine the graph smoothness constraint and the physical decoder.

lattice, causing a shift in its peak along the q axis. How to appropriately model such peak shifting is a critical part of phase mapping algorithms. In DRNets and some other phase mapping algorithms, [1], [11] the shifting of each phase is modeled by one single multiplicative factor, which only models isotropic expansion and compression of an cubic lattice and is not general enough to model XRD patterns of crystals with lower symmetry structures. This may lead to inaccurate phase labeling. To improve upon this, we update PG-DRNet's decoder with a comprehensive lattice model governed by six lattice parameters. These parameters encompass a, b, and c, describing the lengths of the edges, as well as α, β, and γ, representing the angles between the edges. For a specific family of lattice plane (hkl), the XRD peak location p_i in q space can be calculated by

$$
\begin{aligned}
p_i(h,k,l,a,b,c,\alpha,\beta,\gamma) = \\
\frac{2\pi}{V}\Big(& h^2b^2c^2\sin^2\alpha + k^2a^2c^2\sin^2\beta + l^2a^2b^2\sin^2\gamma \\
&+ 2hkabc^2(\cos\alpha\cos\beta - \cos\gamma) \\
&+ 2kla^2bc(\cos\beta\cos\gamma - \cos\alpha) \\
&+ 2hlab^2c(\cos\gamma\cos\alpha - \cos\beta)\Big)^{\frac{1}{2}}
\end{aligned} \tag{3}
$$

where V is the volume of the unit cell parallelepiped. [12] The neural network is then trained using the sampling schema described in the previous session to predict the shift in the lattice parameters of each phase and subsequently construct the XRD pattern through GMM. This method, while requiring more computing time, is more physically-realistic and imposes more rigorous constraints on the decoder model.

The key components in the PG-DRNet framework are summarized in Figure 5. The graph smoothness constraint plays a vital role in modeling the phase connectivity within the system. By incorporating this constraint, we ensure that neighboring data points have similar phase assignments, leading to a more connected and continuous phase distribution. Additionally, we utilize a physical decoder, which enables us to reconstruct the X-ray diffraction (XRD) patterns based on the identified phases. The physical decoder leverages prior knowledge and captures the structural information embedded in the XRD data, allowing more accurate reconstructions of the observed spectra. Overall, the combination of the graph smoothness constraint and the physical decoder form a robust framework that not only captures the phase connectivity but also enables us to interpret and analyze the underlying structural properties of the materials.

IV. Results

We conducted evaluations of PG-DRNet on four distinct material systems characterized by varying element compositions, annealing time, and peak annealing temperature. Our approach successfully models the phase connectivity constraint, resulting in a more accurate representation of the phases' distribution. We also observe improvement in the reconstruction loss, indicating the effectiveness of our methodology in accurately reconstructing the observed spectra.

A. Al-Li-Fe system

We evaluate the performance of PG-DRNet on a synthetic benchmark dataset based on the Al–Li–Fe oxide system. The results are presented in Figure 6. This system has a collection of 231 X-ray diffraction (XRD) patterns representing different compositions, with a total of 158 prototypes. The prototypes exhibit considerable signal overlap, posing a challenging task for manual analysis. PG-DRNet effectively identifies 6 distinct phases across 9 different regions, and the presence of each phase is confirmed through ground truth verification. Notably, PG-DRNet utilized only 421 sub-graphs, whereas the original DRNets employed 100,000 paths during training. This reduction in training samples significantly decreased the training time. Previously, training a single epoch with DRNets consumes over 2 hours. In contrast, the training time for PG-DRNet has been dramatically reduced to approximately 2 minutes. Table I provides a summary of the performance of different models on Al-Li-Fe system:

The original DRNets model achieves a reconstruction loss of 0.038. It successfully identifies 6 distinct phases without any discontinuous regions. The training process involves 10,000 epochs, averaging 11.64 seconds per epoch. On the other hand, when using the DRNets model with Smoothness only, the reconstruction loss improves to 0.033. Similar to the original model, it discovers 6 distinct phases without any discontinuous regions. The training process consists of 50 epochs, with an average duration of 13.82 seconds per epoch.

In comparison, the PG-DRNet model achieved the lowest reconstruction loss of 0.027. It also identifies 6 distinct phases, without encountering any discontinuous regions. The training process took 50 epochs, averaging 10 minutes per epoch. Overall, PG-DRNet improves performance in terms of reconstruction loss and reduces the training time.

B. Bi-Cu-V-oxide system

We extend our evaluation by testing PG-DRNet on the Bi-Cu-V oxide system, and the corresponding results are presented in Figure 7. This system consists of a collection of 307 X-ray diffraction (XRD) patterns with 100 prototypes. Similarly to the previous systems, the prototypes in this system exhibit significant signal overlap, making it challenging to solve using manual analysis alone.

PG-DRNet successfully identifies 15 distinct phases in 19 different mixes within Bi-Cu-V system. The presence of each phase was confirmed through manual examination. Remarkably, PG-DRNet utilizes only 921 sub-graphs, while the original DRNet requires 100,000 paths. This reduction in the number of training samples significantly reduced the training time. Previously, training a single epoch using DRNets could take over 2 hours, whereas with PG-DRNet, it now takes approximately 3 minutes. This reduction in training time enhances the efficiency and scalability of the model, allowing for faster analysis and exploration of phase behavior in complex oxide systems. Similarly to Al-Li-Fe system, the incorporation of graph smoothness with a physical decoder in Bi-Cu-V-oxide system also leads to a lower reconstruction loss, as demonstrated in Table II. The phases in Bi-Cu-V-oxide system includes anisotropic strains in the lattice and thus can only be well-fitted by the new physical-realistic decoder in PG-DRNet, leading to much lower reconstruction loss. These results further highlight the significance of incorporating both physical knowledge and graph smoothness in achieving better results for systems with varying compositions.

C. Bi-O system

To further assess the performance of PG-DRNet, we investigate the Bi-O system to explore its behavior under different annealing times and temperatures, which is carried out by a lateral-gradient laser spike annealing technique. [3] Unlike the Al-Li-Fe or Bi-Cu-V-oxide systems, the Bi-O oxide system has the same composition but different annealing conditions, providing two degrees of freedom: annealing time and peak annealing temperature.

Figure 8 presents our results for Bi-O system. By increasing the graph smoothness weight α from 0.001 to 0.05, we observed a greater connectivity in the phase map. This indicates that the smoothness loss incorporated in PG-DRNet effectively enforces the constraint of phase connectivity. In addition, The graph smoothness constraint in the Bi-O system is effective in eliminating unphysical solutions. Figure 8 demonstrates that when the smoothness constraint is low, we observe the presence of melting or amorphous points in the low temperature region (<500 °C). This occurrence is considered unphysical, as the melting process typically takes place under high temperature conditions. However, as we gradually increase the weight of the smoothness constraint from 0.001 to 0.05, the melting phase gradually disappears, resulting in a continuous phase distribution on the time-temperature map. This indicates that the smoothness constraint plays a crucial role in promoting phase connectivity and suppressing unrealistic phase transitions. By imposing a stronger smoothness constraint, the algorithm encourages neighboring points in the Time-Temperature map to have similar phase assignments, leading to a more continuous and physically meaningful phase distribution. This

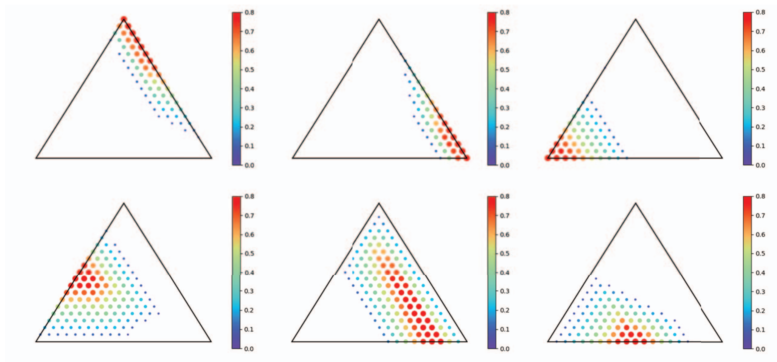

Fig. 6: Activation maps generated by PG-DRNet for Al-Li-Fe oxide system.

	Reconstruction loss	# Discovered Phases	# Discontinuous region	# Training Epochs
DRNets (100K paths)	0.038	6	0	10000 (11.64s per epoch)
PG-DRNet (462 graphs)	**0.027**	6	0	50 (4 min per epoch)
DRNets with Smoothness only (462 graphs)	0.033	6	0	50 (7.35s per epoch)

TABLE I: Different models' performance on Al-Li-Fe system.

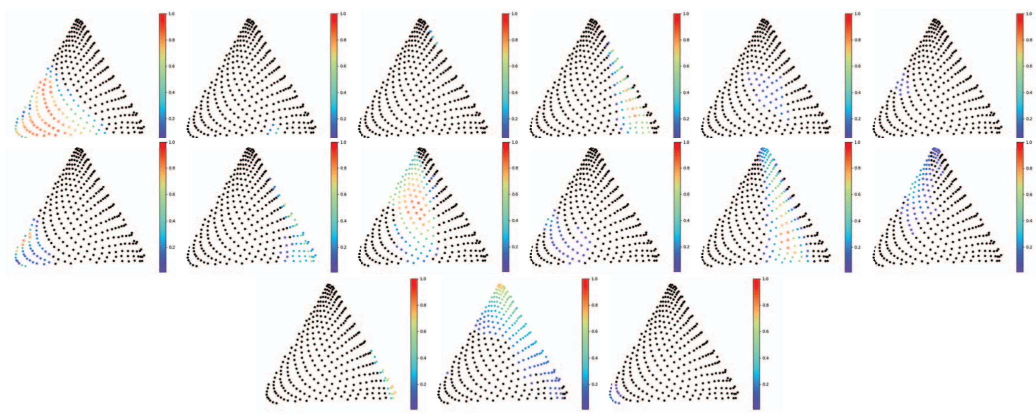

Fig. 7: Activation maps generated by PG-DRNet for the Bi–Cu–V oxide system.

	Reconstruction loss	# Discovered Phases	# Discontinuous region	# Training Epochs
DRNets (100K paths)	3.916	13	0	10000 (13.82s per epoch)
PG-DRNet (921 graphs)	**3.597**	15	0	30 (10 min per epoch)
DRNets with Smoothness only (921 graphs)	4.398	15	0	30 (15.56s per epoch)

TABLE II: Different models' performance on Bi-Cu-V system.

enhancement in the model's performance further demonstrates the effectiveness of PG-DRNet in accurately capturing and representing complex phase behaviors. We further compare the PG-DRNet activations with the ground truth solutions. For Delta and Beta phases, we observe mean absolute errors (MAE) of 0.0965, and 0.0723, respectively.

D. *Ta-Sn-Co-O system*

Previous results have shown that PG-DRNet achieves better performance in material systems with varying compositions or different time and temperature. In addition, we investigate the Ta-Sn-Co-O system, which raises additional challenges due to its four degrees of freedom. The presence of multiple compositional variations (Ta, Sn, Co composition) and distinct time-temperature conditions makes manual analysis extremely challenging in this system.

The Ta-Sn-Co-O system consists of 96 XRD patterns. To effectively analyze this system, we sampled 288 sub-graphs of varying sizes. Our results are shown in Table IV.

PG-DRNet with the physical decoder obtains the lowest reconstruction loss of 3.111, discovering 4 distinct phases without encountering any discontinuous regions. Additionally, it is noteworthy that utilizing DRNets with 100,000 paths can also yield a relatively close reconstruction loss to that of PG-DRNet. This observation can be attributed to the fact that Ta-Sn-Co-O system has only 96 data points, making

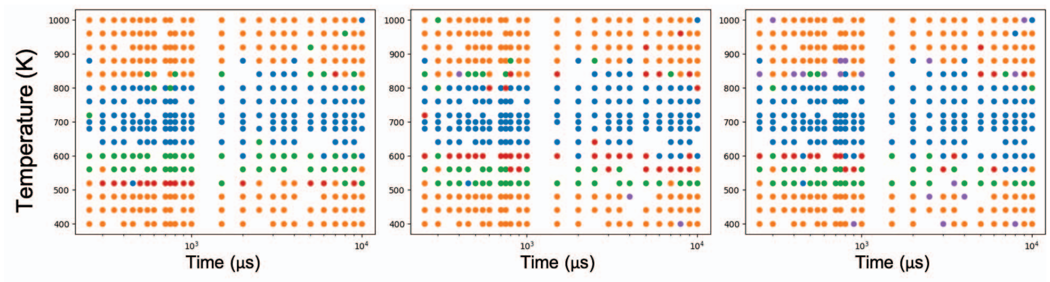

Fig. 8: From left to right: Phase maps with smoothness weight α = 0.05, 0.01 and 0.001. •: Delta + Melting/amorphous; •: Beta; •: Melting/amorphous; •: Beta + Delta; •: Melting only.

	Reconstruction loss	# Discovered Phases	# Discontinuous region	# Training Epochs
DRNets (100K paths)	6.341	4	0	10000 (7.23s per epoch)
PG-DRNet (786 graphs)	**5.342**	4	0	30 (6 min per epoch)
DRNets with Smoothness only (786 graphs)	6.151	4	0	30 (9.34s per epoch)

TABLE III: Different models' performance on Bi-O system.

	Reconstruction loss	# Discovered Phases	# Discontinuous region	# Training Epochs
DRNets (100K paths)	3.251	5	1	10000 (6.43s per epoch)
PG-DRNet (288 graphs)	**3.111**	4	0	50 (1 min per epoch)
DRNets with Smoothness only (288 graphs)	3.854	5	0	50 (4.12s per epoch)

TABLE IV: Different models' performance on Ta-Sn-Co system.

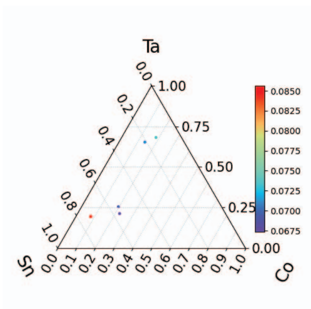

(a) Ta_2O_5 phase distribution in the composition space.

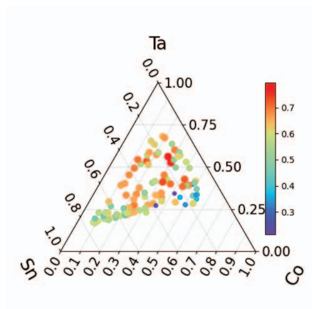

(b) SnO_2 phase distribution in the composition space.

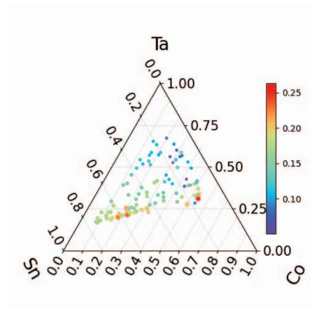

(c) TaO_2 phase distribution in the composition space.

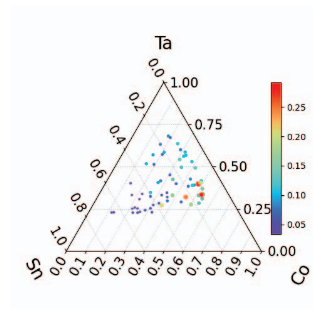

(d) $Co_4Ta_2O_9$ phase distribution in the composition space.

Fig. 9: Activation maps (w.r.t. composition) generated by PG-DRNet for the Ta–Sn–Co-O system.

100,000 paths sufficient for effectively modeling this particular system. However, despite achieving a close reconstruction loss, we observed an additional distinct phase, CoO_2, which does not belong to Ta-Sn-Co-O system when using DRNets with 100,000 paths. This observation highlights limitations of the path-based method in accurately modeling the continuous constraint in such a complex system. The Ta-Sn-Co-O system, with its four degrees of freedom, requires the modeling approach to not only cover all the data points but also capture the connectivity constraint among them. While the path-based method may successfully cover all the points, it falls short in accurately modeling the connectivity constraint, leading to the inclusion of the uncharacteristic phase CoO_2. This emphasizes the advantage of PG-DRNet in capturing the underlying continuous constraints and improving the modeling results in complex systems like Ta-Sn-Co-O. On the other hand, the DRNets with Smoothness only model achieved a reconstruction loss of 3.854, identifying 5 distinct phases while satisfying the continuous constraint. However, it is worth noting that without the inclusion of a physical decoder, we observe the presence of an additional phase, SnO, which does not belong to Ta-Sn-Co-O system. This further highlights that the physical decoder accurately captures the specific phases within a system, avoiding the inclusion of extraneous phases. These findings underscore the importance of integrating physical knowledge and graph smoothness to enhance the analysis and understanding of complex phase behaviors in materials science systems with varying compositions and time-temperature conditions. We further compare the PG-DRNet activations with the ground truth solutions. For Ta_2O_5, SnO_2,

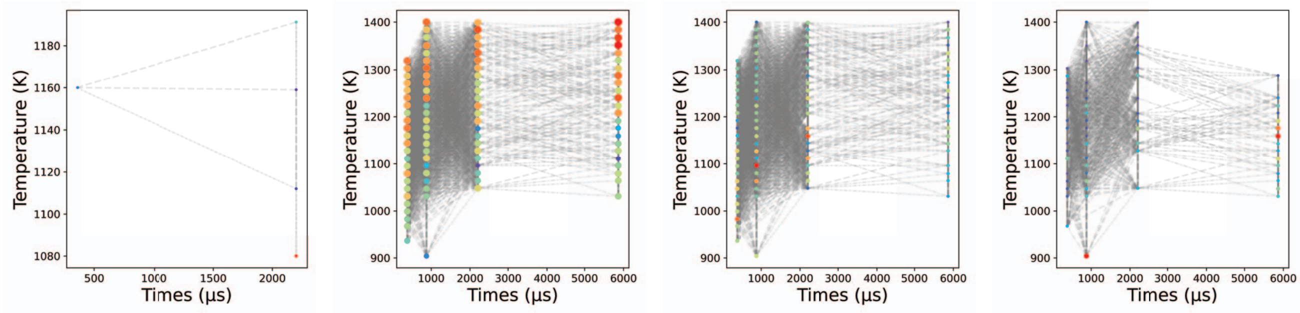

(a) Ta_2O_5 phase distribution in the time-temperature space.

(b) SnO_2 phase distribution in the time-temperature space.

(c) TaO_2 phase distribution in the time-temperature space.

(d) $Co_4Ta_2O_9$ phase distribution in the time-temperature space.

Fig. 10: Activation maps (w.r.t. Time and Temperature) generated by PG-DRNet for the Ta–Sn–Co-O system.

TaO_2, and $Co_4Ta_2O_9$, we observe mean absolute errors (MAE) of 0.0850, 0.0523, 0.0776, and 0.0233, respectively.

V. Conclusion

In this paper, we introduce PG-DRNet, a novel approach for phase mapping in materials science. PG-DRNet incorporates two key novel components: graph smoothness and a physical decoder. The graph smoothness component models the connectivity of the phase field by ensuring similar phase assignments for neighboring data points. This promotes a more connected and continuous phase distribution. The physical decoder captures the structural information of the identified phases, enabling more accurate reconstructions of X-ray diffraction patterns and phase assignments. Additionally, PG-DRNet demonstrates computational efficiency by reducing the number of required training samples, making the phase mapping process more efficient.

Through the comprehensive analysis of material systems characterized by varying compositions, annealing time, and peak annealing temperature conditions, we have evaluated the effectiveness of PG-DRNet. Our findings demonstrate that PG-DRNet effectively captures the phase connectivity within complex systems, resulting in a more connected and continuous phase distribution. Additionally, the integration of a physical decoder has enhanced our ability to accurately reconstruct X-ray diffraction (XRD) patterns.

Overall, by combining the graph smoothness component and the physical decoder, PG-DRNet offers a new framework for solving the phase mapping problem. The proposed approach enhances our ability to study and understand complex phase behaviors in materials science, providing insights into phase connectivity and accurate reconstructions of experimental data. PG-DRNet holds significant potential for advancing materials research and development by enabling more accurate phase mapping and characterization.

Acknowledgement This project is partially supported by the Eric and Wendy Schmidt AI in Science Postdoctoral Fellowship, a Schmidt Futures program; the National Science Foundation (NSF) and the National Institute of Food and Agriculture (NIFA); the Air Force Office of Scientific Research (AFOSR); the Department of Energy; and the Toyota Research Institute (TRI).

References

[1] D. Chen, Y. Bai, S. Ament, W. Zhao, D. Guevarra, L. Zhou, B. Selman, R. B. van Dover, J. M. Gregoire, and C. P. Gomes, "Automating crystal-structure phase mapping by combining deep learning with constraint reasoning," *Nature Machine Intelligence*, vol. 3, no. 9, pp. 812–822, 2021.

[2] W. F. Maier, K. Stoewe, and S. Sieg, "Combinatorial and high-throughput materials science," *Angewandte chemie international edition*, vol. 46, no. 32, pp. 6016–6067, 2007.

[3] R. T. Bell, A. G. Jacobs, V. C. Sorg, B. Jung, M. O. Hill, B. E. Treml, and M. O. Thompson, "Lateral temperature-gradient method for high-throughput characterization of material processing by millisecond laser annealing," *ACS Combinatorial Science*, vol. 18, no. 9, pp. 548–558, 2016.

[4] J. Gregoire, D. Van Campen, C. Miller, R. Jones, S. Suram, and A. Mehta, "High-throughput synchrotron x-ray diffraction for combinatorial phase mapping," *Journal of synchrotron radiation*, vol. 21, no. 6, pp. 1262–1268, 2014.

[5] C. P. Gomes, J. Bai, Y. Xue, J. Björck, B. Rappazzo, S. Ament, R. Bernstein, S. Kong, S. K. Suram, R. B. van Dover *et al.*, "Crystal: a multi-agent ai system for automated mapping of materials' crystal structures," *MRS Communications*, vol. 9, no. 2, pp. 600–608, 2019.

[6] Y. Xue, J. Bai, R. Le Bras, R. Bernstein, J. Bjorck, L. L. L. Longpre, S. Suram, R. van Dover, J. Gregoire, and C. Gomes, "Phase-mapper: an ai platform to accelerate high throughput materials discovery," in *Proceedings of the AAAI Conference on Artificial Intelligence*, vol. 31, no. 2, 2017, pp. 4635–4642.

[7] A. Ludwig, "Discovery of new materials using combinatorial synthesis and high-throughput characterization of thin-film materials libraries combined with computational methods," *NPJ Computational Materials*, vol. 5, no. 1, p. 70, 2019.

[8] R. LeBras, T. Damoulas, J. M. Gregoire, A. Sabharwal, C. P. Gomes, and R. B. Van Dover, "Constraint reasoning and kernel clustering for pattern decomposition with scaling," in *International Conference on Principles and Practice of Constraint Programming*. Springer, 2011, pp. 508–522.

[9] A. G. Kusne, D. Keller, A. Anderson, A. Zaban, and I. Takeuchi, "High-throughput determination of structural phase diagram and constituent phases using grendel," *Nanotechnology*, vol. 26, no. 44, p. 444002, 2015.

[10] V. Stanev, V. V. Vesselinov, A. G. Kusne, G. Antoszewski, I. Takeuchi, and B. S. Alexandrov, "Unsupervised phase mapping of x-ray diffraction data by nonnegative matrix factorization integrated with custom clustering," *npj Computational Materials*, vol. 4, no. 1, p. 43, 2018.

[11] S. K. Suram, Y. Xue, J. Bai, R. Le Bras, B. Rappazzo, R. Bernstein, J. Bjorck, L. Zhou, R. B. Van Dover, C. P. Gomes *et al.*, "Automated phase mapping with agilefd and its application to light absorber discovery in the v–mn–nb oxide system," *ACS combinatorial science*, vol. 19, no. 1, pp. 37–46, 2017.

[12] B. D. Cullity and S. R. Stock, *Elements of X-ray Diffraction.* Pearson, 2014.